Polymer Bulletin
https://doi.org/10.1007/s00289-024-05472-x

ORIGINAL PAPER

Enhancing optical properties and antimicrobial efficacy of PEO/CS-doped TiO_2 nanoparticles for food packaging applications

Azzah M. Alghamdi[1] · I. Guizani[2] · E. M. Abdallah[3] · M. O. Farea[4] · M. A. Morsi[5,6] · Ibrahim A. Alhagri[7] · Talal F. Qahtan[8] · Ahmed N. Al-Hakimi[7] · Sadeq M. Al-Hazmy[7] · S. El-Sayed Saeed[7] · Abuzar E. A. E. Albadri[7]

Received: 27 November 2022 / Revised: 22 August 2023 / Accepted: 24 June 2024

Abstract

Utilizing the solution casting technique, polymer nanocomposites (PNCs) films including polyethylene oxide and chitosan (PEO/CS) doped with titanium dioxide nanoparticles (TiO_2 NPs) as nanoceramic were successfully synthesized. The study investigated how varying TiO_2 nanoparticle concentrations influenced the structural, optical properties, and antibacterial activity of the polymeric matrix. XRD patterns revealed an increase in the amorphous nature of the polymer blend as the content of TiO_2 NPs inside the PEO/CS blend grew. The FT-IR analysis confirmed the interaction between TiO_2 NPs and the PEO/CS blend. This confirmation is attributed to the observed vibrational changes upon the incorporation of TiO_2 dopant into the polymer matrix. The UV–visible spectrum aided in the determination of optical energy band gaps (both direct and indirect), showing reductions in both E_{gd} and E_{gin} with higher TiO_2 concentrations. SEM highlighted the partial compatibility between PEO/CS and TiO_2, while transmission electron microscopy depicted spherical TiO_2 NPs with diameters ranging from approximately 9 to 25 nm. Antimicrobial assessments indicated heightened efficacy in all nanocomposite samples compared to the pure PEO/CS composite, with a linear correlation to the quantity of TiO_2 nanoparticles present. These findings strongly suggest the potential of these nanocomposites for food packaging applications.

Keywords PEO · CS · Antibacterial activity · FT-IR · TEM · Food packaging

Extended author information available on the last page of the article

Published online: 24 August 2024

Introduction

Blending more than one polymers involves creating a blend that incorporates the favorable properties of each polymer within the blend [1, 2]. The effectiveness of this procedure in producing novel materials with diverse properties is widely acknowledged. Furthermore, it enables these materials to gain additional attributes such as enhanced flexibility, usability, and cost efficiency [3, 4]. The applications of many synthetic polymers hinge on the delicate balance between their resistance and biodegradability. Studying polymer biodegradation has become crucial, as bacterial and fungal attacks on polymers remain relatively unexplored. In recent times, biomaterials derived from natural sources have gained prominence due to their numerous benefits, including biocompatibility, non-toxicity, and biodegradability [5]. Chitosan (CS), derived from abundant and cost-effective sources such as crustacean shells, possesses inherent antibacterial and antifungal properties [6]. This makes it a versatile foundation for various applications. Latest articles have heavily focused on tackling the issue of biological degradation of valuable materials, aiming to utilize chitosan as an environmentally friendly solution in diverse industries [7]. An exemplary case involves the utilization of reliable polymeric systems with biocidal characteristics to safeguard materials like food packaging, paints, and pharmaceutical products against deterioration [8].

While chitosan possesses numerous interesting characteristics, its utilization is hampered by drawbacks like low crystallinity, inadequate thermal stability, and mechanical fragility [9]. Additionally, its poor solubility and loosely cationic nature restrict its practical use in antibacterial applications [10]. To address these limitations, a transformative approach involves integrating chitosan into hydrogels and aerogels, augmented by the incorporation of metal oxide nanoparticles. This combination enhances the antibacterial effectiveness of polymer blends, particularly in the case of PEO/CS. The addition of metal oxide NP to the polymeric mixture serves to amplify various material attributes, encompassing structural, chemical, physical, optical, swelling, and antibacterial properties [11–13]. Metal oxide nanoparticles have attracted global attention due to their economical production, limited human toxicity, antibacterial properties, and inertness to chemicals and biology [14]. Titanium dioxide nanoparticles (TiO_2 NPs) find broad application across various biomedical domains because of their significant anticancer, antifungal, and antibacterial properties [15]. Polyethylene oxide (PEO) stands out as a rare biodegradable synthetic polymer authorized for internal use in sectors such as cosmetics, food, and personal care products [16]. Chitosan and polyethylene oxide are currently gaining prominence in various technologies, thanks to their notable attributes including easy processability, favorable thermal properties, and cost-effectiveness. PEO, in particular, finds diverse applications owing to its commendable biocompatibility and minimal toxicity, making it well-suited for various fields [16].

Nanoparticles exhibit remarkable antimicrobial properties due to the generation of reactive oxygen species, leading to the eventual demise of bacterial cells [17]. Antimicrobial packaging is achieved by incorporating commonly used nanoparticles such as TiO_2, CuO, ZnO, and Ag into chitosan films [18, 19]. Incorporating

nanoparticles enhances the gas barrier, antimicrobial attributes, and heat resistance of CS samples. Archana et al. [20] introduced nanocomposite composed of CS, PVP, and TiO_2 for potential use as wound dressing materials, conducting in vitro assessments. They also explored CS, PVP, and Ag films, investigating both in vitro and in vivo scenarios to investigate wound healing [21]. Lin et al. [7] developed a gelatin-CS/TiO_2-Ag nanocomposites designed for food packaging application. Their study focused on assessing antimicrobial effects against both Gram-positive and Gram-negative bacteria. Nanomaterials, due to their fine particle size and substantial specific surface areas, show promise as reinforcing agents, contributing to improved microstructure, antibacterial activity, and electrical properties in nanocomposites [22]. The incorporation of these nanomaterials leads to heightened chemical reactions within composites, exerting a substantial influence on their overall efficiency. Despite this, only limited research has investigated the effects of nanoparticles on the efficiency attributes of reinforced nanocomposites. The introduction of fillers has been observed to elevate ionic conductivity, antibacterial effectiveness, and thermal stability within the polymer blend [23]. TiO_2 nanoparticles (NPs) stand out due to their remarkable qualities, such as strong antibacterial effectiveness, chemical stability, biocompatibility, and exceptional photocatalytic performance [24]. When subjected to ultraviolet (UV) radiation, electron–hole pairs are generated on the surface of TiO_2 nanoparticles due to their specific band gap energy. As a result, these electrons can be harnessed to combat bacteria. Notably, TiO_2 possesses strong UV-blocking capabilities, making it potentially valuable for food preservation purposes [25]. Zhang et al. [26] crafted CS/TiO_2 bionanocomposite films, investigating their antibacterial effectiveness through UV irradiation. Incorporating TiO_2 nanoparticles into the CS matrix led to improved properties of the bionanocomposite films, including enhanced wettability, amplified antibacterial activity (under UV irradiation), and fortified mechanical characteristics. By introducing dopant nanoparticles (NPs), the reduction of surface energy in TiO_2 NPs became feasible. As a result, this approach offered a solution to circumvent the agglomeration of TiO_2 NP within the polymer blend [27]. Until now, there has been a notable absence of efforts to create nanocomposites incorporating PEO, CS, and TiO_2 NPs. Consequently, the focal point of this study is to introduce PEO/CS-TiO_2 bionanocomposites, which are both economical and straightforward to synthesize, and possess environmentally friendly characteristics. These bionanocomposites exhibit antibacterial properties, making them suitable for applications in food packaging.

Experimental work

Chemical

PEO polymer with a molecular weight (M.W.) of 35,000 g mol^{-1} was sourced from ACROS Organic in Morris Plains, New Jersey. The CS used was obtained from Mallinckrodt USA with a M.W. of 4×10^5 and 96% deacetylation degree. The TiO_2, acquired from Sigma-Aldrich in Germany, boasted a purity level of 98.96%. The

above chemicals were dissolved in double-distilled water purchased from Al-Gomhoria, based in Mansoura, Egypt.

Preparation of PEO/CS-TiO_2 nanocomposites

PEO and CS were separately dissolved in double-distilled water at the necessary amounts to produce the nanocomposites samples. The solutions gradually turned crystal clear and transparent over a span of three hours. The resulting samples were composed of approximately 70% CS and 30% PEO. By dispersing TiO_2 in double-distilled water for two hours, polymer nanocomposites at various weight percentages (0.0%, 4.0%, 8.0%, and 12.0 wt%) were achieved. Subsequently, a thorough mixing of all solutions generated a homogeneous, viscous liquid. This liquid was cast into a petri dish, and as the solvent gradually evaporated over three days, the polymer blend transformed into nanocomposite. These PEO/CS-TiO_2 nanocomposites were carefully peeled from the petri dish and utilized for subsequent investigations.

Characterization

The films with varying TiO_2 concentrations underwent XRD diffraction analysis via DIANO-XRD 800 diffractometer, employing Ni filter Cu Kα radiation with a wavelength of $\lambda \approx 1.542$ nm. Determination of functional groups in PEO/CS-TiO_2 nanocomposites was conducted through FT-IR spectroscopy using a Nicolet iS10 instrument from the USA. UV/Vis spectra of the polymeric samples were recorded at RT using a JASCO UV/VIS spectrophotometer (Model V/630, Japan). The size and shape of TiO_2 NPs were explored using TEM (JEOL JEM-1011, Japan). Furthermore, the surfaces of the formed thin films were investigated via scanning electron microscopy (SEM) (JEOL JSM-6510 LV, USA).

Results and discussion

XRD analysis

X-ray diffraction is a valuable method used to determine the structure of materials. The XRD spectra for PEO, CS, and PEO/CS blend are shown in Fig. 1. The spectral distribution of CS reveals its amorphous character through a notable broad peak centered at approximately $2\theta = 21.28°$. The semicrystalline nature of PEO is evidenced by the presence of three distinct sharp peaks in its spectrum, located at $2\theta = 18.88°$, 23.65°, and 26.15°. These peaks correspond to crystallographic planes (120), (112), and (121), highlighting the ordered structural pattern within PEO [28]. Figure 2 presents the X-ray diffraction for PEO/CS and its nanocomposite incorporating TiO_2 NP. The XRD spectra reveal the composite's semicrystalline nature, with notable strong peaks observed at 18.88° and 23.65°. These peaks stem from the semicrystalline of PEO present in the complex. In the XRD patterns of the nanocomposite sample, several low-intensity peaks are evident at $2\theta = 32.50°$, 36.01°, 39.53°,

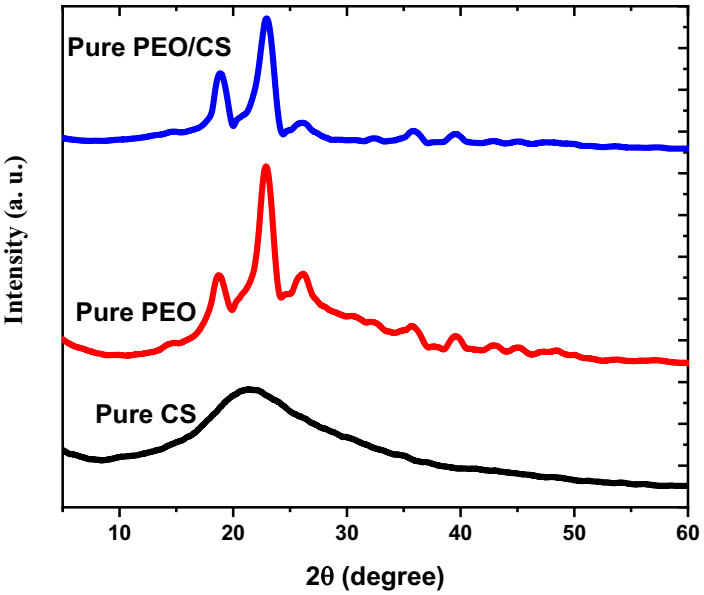

Fig. 1 XRD patterns of CS, PEO, and PEO/CS composite

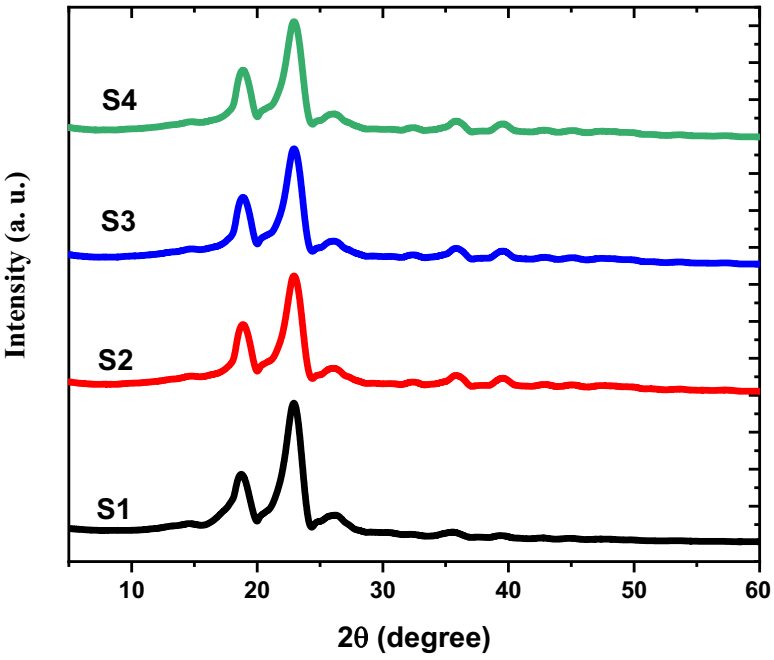

Fig. 2 XRD patterns of PEO/CS composite and PEO/CS filled with different concentrations of TiO_2 NPs

and 42.54°. Notably, the two primary peaks exhibit a decrease in intensity and a broadening of their width. The findings suggest a randomized distribution of TiO_2 within the PEO/CS chain, a conclusion supported by strong interactions between the PEO/CS polymeric matrix and TiO_2, as indicated by FT-IR measurements [29]. This interaction leads to a decrease in the nanocomposite's degree of crystallinity and an increase in the amount of amorphous areas. Interestingly, the X-ray diffraction for the prepared samples do not reveal any new peaks, signifying the complete dissolution of TiO_2 nanoparticles within the PEO/CS blend.

FT-IR spectra

An FT-IR analysis is undertaken to investigate the interaction between the titanium dioxide and polymer blend within the nanocomposites. Figure 3 illustrates the distinctive spectral features that distinguish between the pristine PEO/CS samples and the PEO/CS-TiO_2 NPs nanocomposite samples. Table 1 presents the wavenumbers associated with notable peaks and their corresponding assignments for these samples. Within the PEO/CS polymeric matrix incorporating titanium dioxide nanoparticles, the simultaneous occurrence of (OH, C=O) groups in CS and (C–O–C) groups in PEO points toward the compatibility and miscibility of the blended sections. PEO exhibits a notable aptitude for establishing intermolecular hydrogen

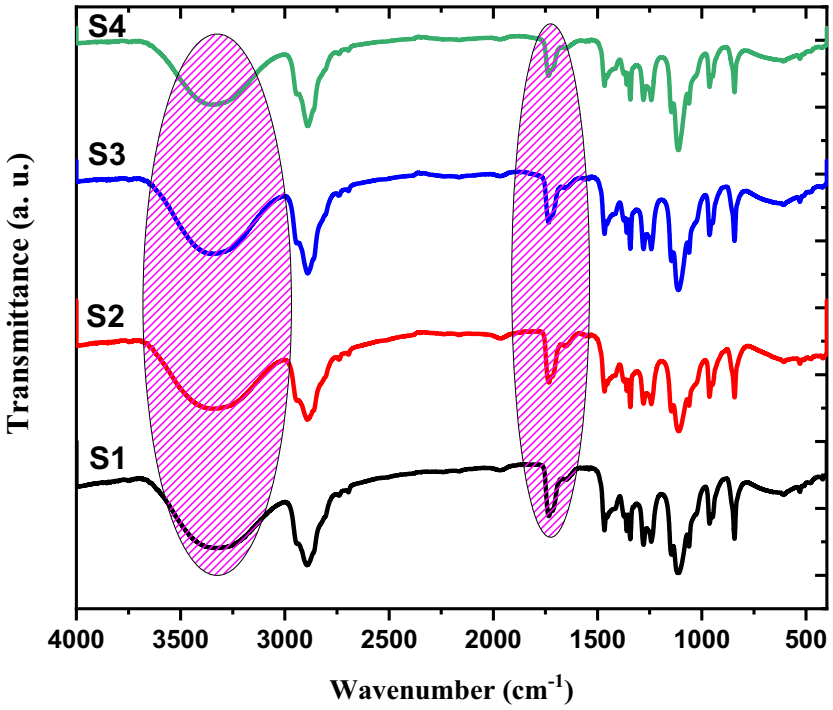

Fig. 3 FT-IR spectra of PEO/CS composite and PEO/CS doped with various concentrations of TiO_2 NP

Table 1 FT-IR of the vibrational assignment for the samples under investigation

Wavenumber (cm^{-1})	Assignment
3328	O–H stretching
2939	CH asymmetric stretching of CH_2
1726	C=O stretching
1431	C–C stretching
1089	Symmetric and asymmetric C–O–C stretching
1067	C–O stretch
963	CH bending mode
838	CO stretching

bonds, especially with highly electronegative substances. The presence of electronegative oxygen and hydroxyl groups within CS polymers suggests their exceptional role as proton acceptors in these interactions [30]. In the FT-IR spectra of the pure blend, a broad bandwidth is evident at 3328 cm^{-1}, indicating the presence of O–H stretching vibrations within the mixture.

In the pristine PEO/CS samples, distinct transmittance peaks emerge at specific wavenumbers: 2939 cm^{-1}, linked to $–CH_2$ asymmetric stretching and –CH asymmetric stretching; 1726 cm^{-1}, corresponding to amide C=O stretching; 1431 cm^{-1}, associated with C–C stretching and $–CH_3$ bending; and 1067 cm^{-1}, indicative of C–O stretching and vibration [31]. Distinctive transmittance bands at 963 cm^{-1} and 838 cm^{-1} arise from the CH bending mode and C–O stretching, respectively, representing typical features of pure PEO. Upon introducing the nanofiller (TiO_2 NPs), the hydroxyl band at 3328 cm^{-1} noticeably widens. Additionally, the presence of TiO_2 NPs in PEO/CS nanocomposites induces slight shifts and changes in the intensity of the band at 1726 cm^{-1}, as depicted in Fig. 3. These findings imply a robust interaction between the PEO and CS, as illustrated in Scheme 1.

Optical properties

UV/Vis analysis involves measuring how much UV and visible light is absorbed or reflected by a sample, providing information about its composition and the concentration of absorbing or reflecting substances [32]. The absorption spectra for PEO/CS composite and PEO/CS filled with various TiO_2 NP concentrations are shown in Fig. 4. The absorption edge noticed at 273 nm in the PEO/CS spectrum can be attributed to the $n \rightarrow \pi^*$ transition. Additionally, there is another distinct peak corresponding to $\pi \rightarrow \pi^*$ transition, positioned at 385 nm [33]. As the concentration of TiO_2 increases, the intensity of the peak at 273 nm grows stronger, and it undergoes a shift toward longer wavelengths (redshift). XRD analysis indicates that this shift could be attributed to alterations in crystallinity, suggesting possible complexation or homogeneity changes. Moreover, variations in band gaps between the polymer

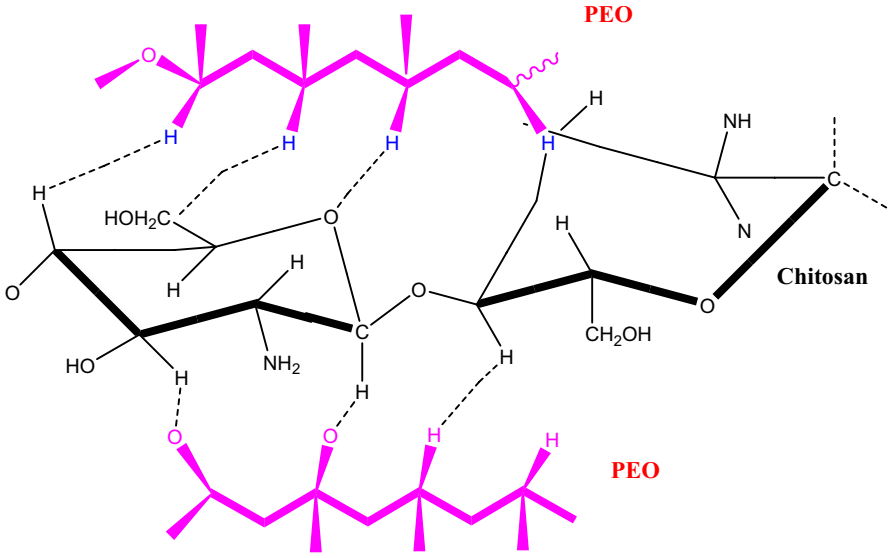

Scheme 1: The possible mechanism for interaction between CS and PEO

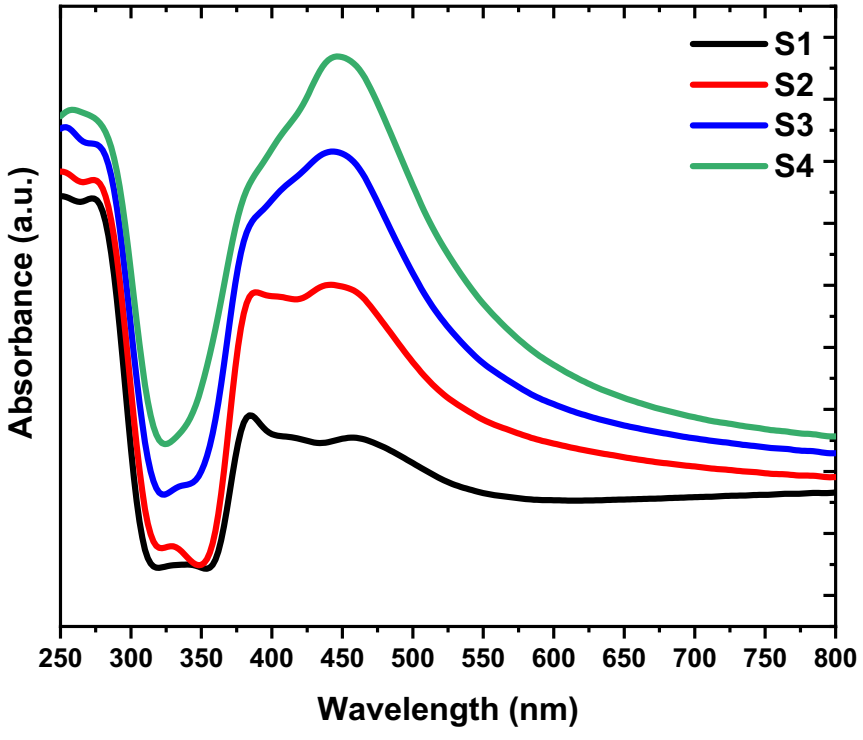

Fig. 4 Absorption spectra of PEO/Cs blend and PEO/Cs filled with various concentrations of TiO_2 NP

composite and TiO_2 NP could also contribute to this observed phenomenon [34, 35]. In the prepared films, a distinctive peak emerges at 460 nm, which is indicative of the surface plasmon resonance (SPR) of the titanium nanoparticles. This observation suggests the presence of titanium nanoparticles within the PEO/CS matrix, as further supported by the detection of an SPR peak. Notably, there is an enhancement in the position of SPR peak and a shift toward longer wavelengths. To validate their interaction and complexation, a modified mixture of PEO/CS and TiO_2 was utilized. The energy gap (E_g) is calculated using the following equation [36, 37]:

$$(\alpha hv) = D(hv - E_g)^r \tag{1}$$

Here "hv" represents the photon energy, and "D" stands for the constant. The value of "r" varies based on whether the electronic transition is direct or indirect. For direct transitions, "r" is 2, while for indirect transitions, it takes a value of 1/2 in the k space. An absorption coefficient (α) can be calculated using the Beer–Lambert's formula [33].

$$\alpha(v) = 2.303\left(\frac{A}{T}\right) \tag{2}$$

Here "A" represents absorbance, and "T" stands for the thickness of the films under investigation. Figures 5 and 6 illustrate the graphs of $(\alpha h\nu)^2$ and $(\alpha h\nu)^{1}/^{2}$ as functions of $h\nu$ for both the PEO/CS composite and the PEO/CS composite filled with varying concentrations of TiO_2 nanoparticles. The values for the direct and indirect energy gaps (E_g) are revealed in Table 2. The optical band gap values E_g

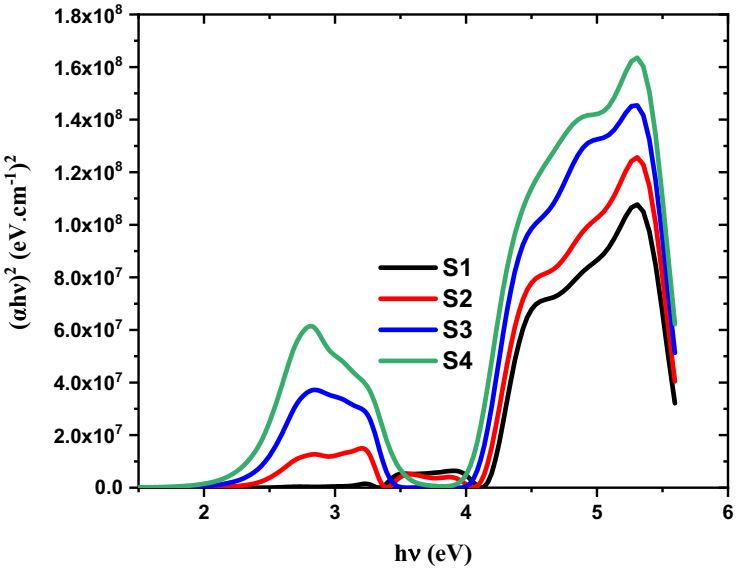

Fig. 5 Plot of $(\alpha hv)^2$ versus hv of PEO/Cs composite and PEO/Cs doped with different concentrations of TiO_2 NPs

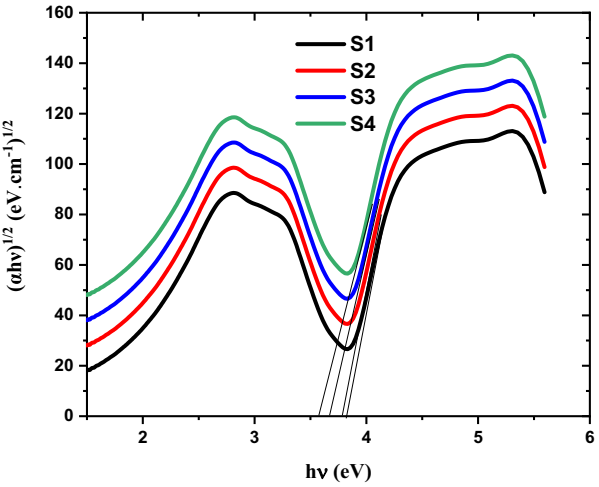

Fig. 6 Plot of $(\alpha h\nu)^{1/2}$ versus $h\nu$ of PEO/Cs blend and PEO/Cs doped with different concentrations of TiO_2 NPs

Table 2 Values of direct and indirect energy gaps for all samples under investigation

Description	Filler concentration (TiO_2 NPs) %	E_g (eV)	
		Direct	Indirect
S1	0.00	4.22	3.79
S2	4.0	4.13	3.76
S3	8.0	4.02	3.66
S4	12.0	3.94	3.56

decrease as filler concentrations increase from 4.0 to 12.0 wt%, as shown in Table 2. The energy gap values for direct transitions decreased from 4.22 to 3.94 eV, while the energy gap values for indirect transitions decreased from 3.79 to 3.56 eV. The decrease in energy gap values is attributed to the introduction of TiO_2 nanoparticles, which create localized states within the material. These localized states offer additional electronic pathways, facilitating easier electronic transitions and contributing to the observed reduction in energy gap values. Consequently, these changes in the material's electronic structure lead to alterations in its optical properties.

TEM image of TiO_2 NPs

Transmission Electron Microscopy (TEM) is a cutting-edge imaging method employed in materials science and nanotechnology for observing intricate structural details at the nanometer scale. The shape and size of the resulting nanoparticles are depicted in Fig. 7. Figure 7a illustrates the characterization of TiO_2 nanoparticles through a Transmission Electron Microscopy (TEM) image, fabricated using the sol–gel technique. Figure 7b demonstrates the nanoparticle size distribution,

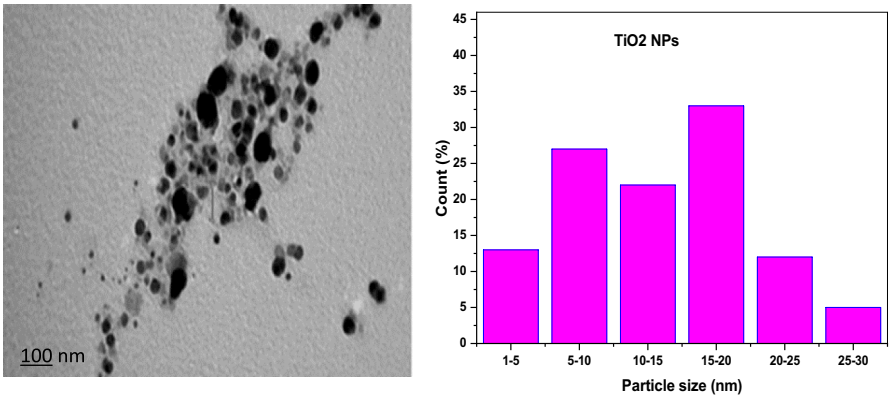

(a) (b)

Fig. 7 **a** TEM image TiO_2 NPs and **b** the corresponding histograms of TiO_2 NPs

presented through a histogram. The TEM image clearly shows the formation of nanoscale titanium oxide grains. These grains exhibit a uniform distribution in terms of grain size, appearing as spherical particles with diameters ranging from approximately 9 to 25 nm. Furthermore, a relatively consistent sample was created, displaying a collection pattern of TiO_2 NP. Notably, this system's TEM images reveal the absence of aggregate formation while depicting the nanoparticles' distribution.

SEM images

Figure 8 depicts the distinctive SEM images of the PEO/CS polymer blend infused with varying concentrations of TiO_2 nanoparticles. In particular, Figure 8a portrays the surface of the PEO/CMC polymer blend, characterized by its smoothness and the presence of regularly distributed spherical pores. Upon introducing TiO_2 nanoparticles into the polymer blend, these pores experience partial filling, as observed in Figure 8b–d. A comparison to the pure PEO/CS sample reveals that at a TiO_2 content of 4.0 wt%, the pores are smaller, while for the 12.0 wt% sample, the surface becomes coarser due to extensive nanoparticle pore filling. Consequently, the addition of TiO_2 significantly influences the surface morphology of the PEO/CS composite. This phenomenon suggests a noteworthy interplay between metal oxides and organic materials. Of particular interest is the absence of evident phase separation in the images. This observation underscores the effective interaction between the PEO/CS matrix and TiO_2 nanoparticles. It provides clear evidence of the acceptable complexation between these components, indicating their successful integration.

Antibacterial studies

Figure 9a–c presents the results of an in vitro activity index assay conducted on collected samples against three bacterial strains: *Pseudomonas aeruginosa*, *Escherichia*

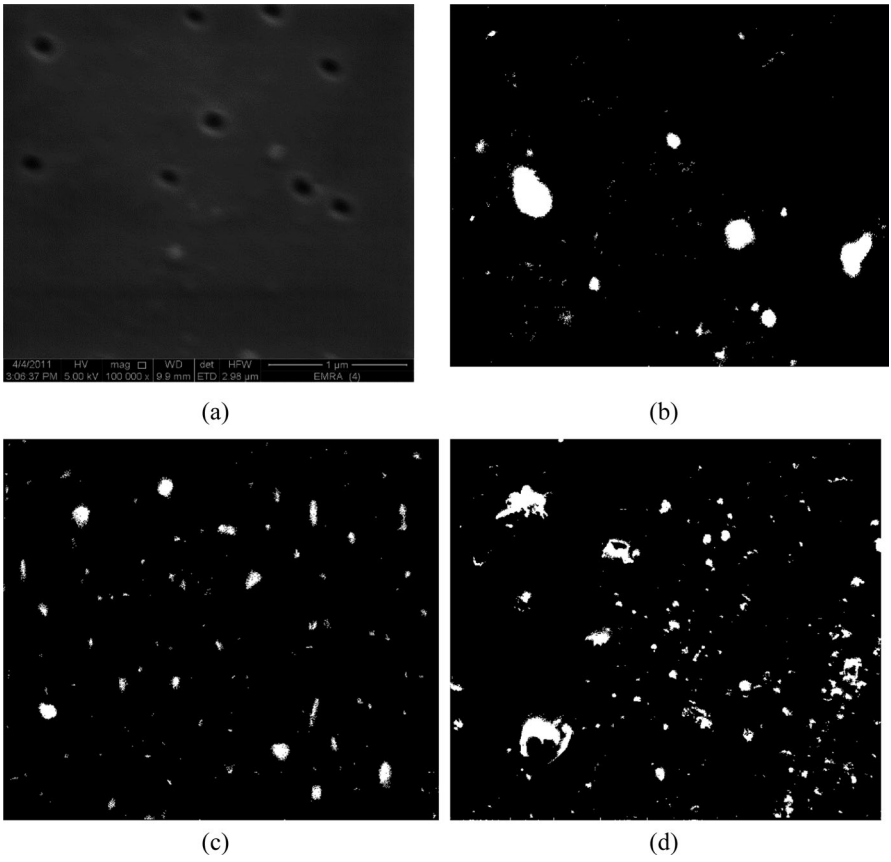

Fig. 8 SEM images of **a** PEO/CS polymer blend, **b** PEO/CS-4.0% TiO_2, PEO/CS-8.0% TiO_2, and PEO/CS-12.0% TiO_2 NPs

coli, and *Staphylococcus aureus*, which were used as control organisms. The findings revealed a consistent increase in antibacterial activity as the concentration of TiO_2 NPs in the samples increased. Notably, the study identified broad-spectrum antimicrobial effects during the investigation. Elevating the concentration of TiO_2 NPs was found to enhance the antibacterial activity against the targeted bacterial species, with *Pseudomonas aeruginosa* exhibiting the most pronounced response in the antibacterial assay. The bacterial species present in the films were observed on agar plates that had been inoculated with the test organisms and subsequently incubated at 35 °C. The resulting data, presented in Table 3, detailed the sizes of inhibition areas (in millimeters) noticed after a 48-h period. These results provided insights into the influence of both pristine PEO/CS and its nanocomposites on the inhibition area and activity index [38]. Across all samples, an increase in the concentration of TiO_2 NPs correlated with a rise in both the diameter of inhibition areas and the activity index. Notably, *Staphylococcus aureus* bacteria exhibited larger inhibition zones and higher activity indices compared to *Escherichia coli*

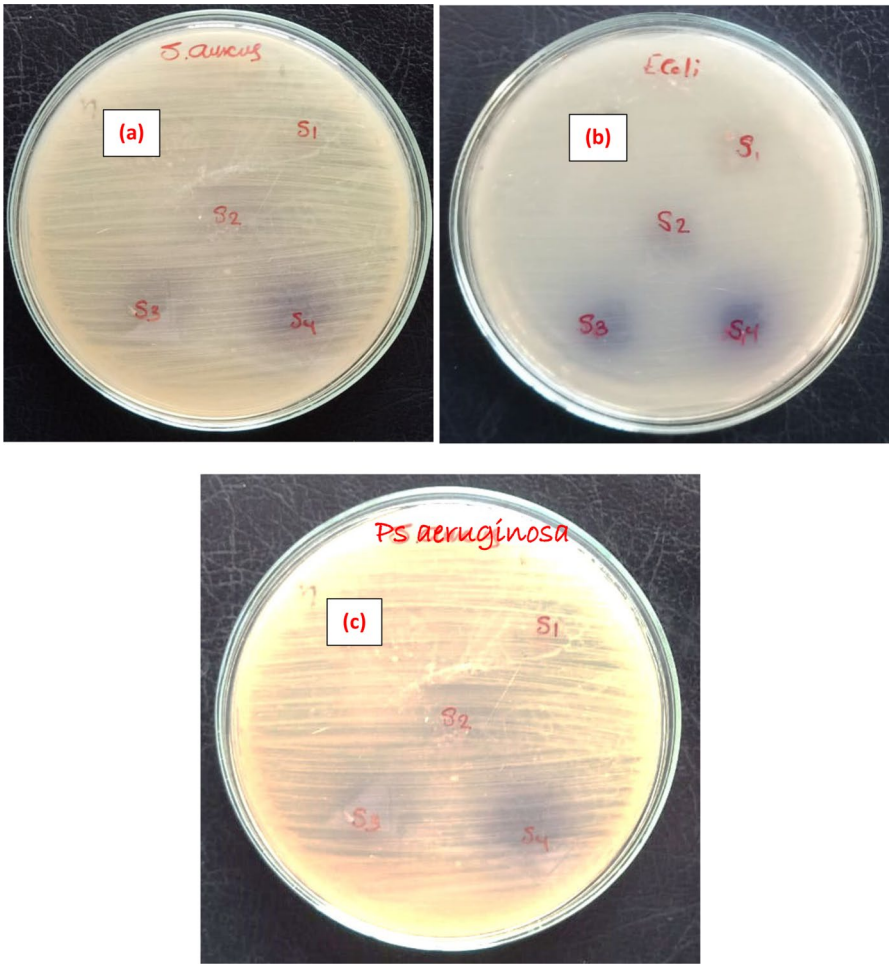

Fig. 9 Antibacterial inhibition zones of PEO/CS blend filled with different concentrations of TiO_2 NPs

Table 3 Antibacterial activity of PEO/CS doped with various concentrations of TiO_2 NPs

Samples	*P. aeruginosa* diameter of area (mg/ml)	*E. coli* diameter of area (mg/ml)	*S. aureus* diameter of area (mg/ml)
S1	3	2	5
S2	8	11	19
S3	13	15	36
S4	16	22	41

and *Pseudomonas aeruginosa* bacteria. The study attributed the inhibition of the examined region to the operation of the Ti ion release mechanism. This mechanism induced variations in bacterial cell permeability, generated reactive oxygen species,

disrupted metabolic processes, and ultimately led to the demise of bacterial cells due to their destruction. The enhanced antibacterial activity of TiO_2 NPs was attributed to their ability to trigger free OH radicals and all H–O–O radicals, owing to their unique chemical properties [39]. The small size of TiO_2 NPs and their capacity to penetrate cell membranes were highlighted as pivotal factors in their biocidal process. Upon interaction with the cellular environment, TiO_2 NPs released reactive species, further contributing to their antibacterial action. The study's findings emphasized the potential of PEO/CS-TiO_2 NP samples as a feasible alternative to synthetic equivalents in the realm of food packaging. This was attributed to the heightened antibacterial activity of TiO_2 NPs, which could enhance food safety by preventing bacterial contamination.

Limitation of work

This study investigated the synthesis of bionanocomposite films containing varying amounts of TiO_2 nanoparticles (NPs), up to a maximum loading of 12 wt%. Scanning electron microscopy (SEM) revealed an increase in TiO_2 NP aggregation on the surface of the nanocomposites at higher loading levels (8 and 12 wt%). Conversely, nanocomposites with lower loadings (0 and 4 wt%) exhibited a more uniform distribution of NPs with minimal aggregation. Interestingly, the highest antibacterial activity was observed for the films containing 4 and 8 wt% TiO_2 NPs. Based on these findings, the optimal loading of TiO_2 NPs appears to be 4 wt%, due to the balance between improved antibacterial activity and reduced aggregation. This finding suggests that bionanocomposite films containing 4 wt% TiO_2 NPs offer the best potential for further evaluation and development.

Conclusion

Polymer composite samples, comprising PEO/CS polymers combined with varying concentrations of TiO_2 NPs, were successfully synthesized via a solution casting method. The structural investigations were conducted to explore both the phenomenon of polymer intercalation and the subsequent alterations in morphological characteristics. XRD analysis unequivocally indicated a reduction in the crystalline nature of the PEO/CS polymer blend. Notably, TEM imaging discernibly captured the spheroidal morphology of TiO_2 nanoparticles, spanning a size spectrum from 9 to 25 nm. FT-IR analysis further validated the creation of polymer mixtures and intricate nanoceramic complexes within the nanocomposites. Meanwhile, UV–Vis spectroscopy distinctly showcased a decline in optical bandgaps, both direct and indirect, as TiO_2 NPs content increased. The hybrid nanocomposite exhibited robust antimicrobial properties, effectively combating both Gram-positive and Gram-negative bacteria. Given its eco-friendly and non-toxic composition, coupled with these augmented attributes, this hybrid nanocomposite holds immense potential in diverse sectors such as biomedicine, packaging, and wrapping, notably within the realm of dynamic food packaging applications.

Author contributions Azzah M Alghamdi, Talal F. Qahtan, and S. El-Sayed Saeed were involved in methodology, formal analysis, investigation, and writing—review and editing. I. Guizani, M.O. Farea, M. A. Morsi, Ahmed N. Al-Hakimi, Sadeq M. Al-Hazmy, and Abuzar EAE Albadri were involved in investigation and writing—review and editing. E. M. Abdallah contributed to methodology, formal analysis, and investigation. Ibrahim A. Alhagri took part in conceptualization, methodology, and writing—review and editing.

Funding This work was funded by the University of Jeddah, Jeddah, Saudi Arabia, under grant No. (UJ-24-DR-2470-1). Therefore, the authors thank the University of Jeddah for its technical and financial support.

Data and materials availability The data that support the findings of this study are available on request from the corresponding author. The data are not publicly available due to privacy or ethical restrictions.

Declarations

Conflict of interest The authors declare that they have no known competing financial interests or personal relationships that could have appeared to influence the work reported in this paper.

Ethical approval This research did not contain any studies involving animal or human participants, nor did it take place on any private or protected areas hence no specific permissions were required.

References

1. Zarei M et al (2021) Fabrication and characterization of conductive polypyrrole/chitosan/collagen electrospun nanofiber scaffold for tissue engineering application. Int J Biol Macromol 168:175–186
2. Al-Muntaser A et al (2024) MoO_3 nanoplates reinforced the structural, electrical, mechanical, and antibacterial characteristics of polyvinyl pyrrolidone/sodium alginate polymer blend for optoelectronics and biological applications. Int J Biol Macromol 254:127894
3. Charles APR et al (2021) Electrohydrodynamic processing of natural polymers for active food packaging: a comprehensive review. Compr Rev Food Sci Food Saf 20(6):6027–6056
4. Chen S, Skordos A, Thakur VK (2020) Functional nanocomposites for energy storage: chemistry and new horizons. Mater Today Chem 17:100304
5. Priyadarshi R, Rhim J-W (2020) Chitosan-based biodegradable functional films for food packaging applications. Innov Food Sci Emerg Technol 62:102346
6. Ragab H et al (2024) Improving the optical, thermal, mechanical, electrical properties and antibacterial activity of PVA-chitosan by biosynthesized Ag nanoparticles: eco-friendly nanocomposites for food packaging applications. Int J Biol Macromol 264:130668
7. Archana D et al (2015) Chitosan-PVP-nano silver oxide wound dressing: in vitro and in vivo evaluation. Int J Biol Macromol 73:49–57
8. Alamry KA et al (2018) Potential anti-cancer performance of chitosan-based β-ketosulfone derivatives. Cogent Chem 4(1):1559435
9. Ulu A et al (2020) Chitosan/polypropylene glycol hydrogel composite film designed with TiO_2 nanoparticles: a promising scaffold of biomedical applications. Int J Biol Macromol 163:529–540
10. Dai F et al (2019) Chitosan-TiO_2 microparticles LBL immobilized nanofibrous mats via electrospraying for antibacterial applications. Int J Biol Macromol 135:233–239
11. Abdeen ZI, El Farargy AF, Negm NA (2018) Nanocomposite framework of chitosan/polyvinyl alcohol/ZnO: preparation, characterization, swelling and antimicrobial evaluation. J Mol Liq 250:335–343
12. Zhou K et al (2022) Hybrid Ag nanoparticles/polyoxometalate-polydopamine nano-flowers loaded chitosan/gelatin hydrogel scaffolds with synergistic photothermal/chemodynamic/Ag+ anti-bacterial action for accelerated wound healing. Int J Biol Macromol 221:135–148

13. Pandian H et al (2023) Azadirachta indica leaf extract mediated silver nanoparticles impregnated nano composite film (AgNP/MCC/starch/whey protein) for food packaging applications. Environ Res 216:114641
14. Farhoudian S, Yadollahi M, Namazi H (2016) Facile synthesis of antibacterial chitosan/CuO bionanocomposite hydrogel beads. Int J Biol Macromol 82:837–843
15. Ziental D et al (2020) Titanium dioxide nanoparticles: prospects and applications in medicine. Nanomaterials 10(2):387
16. Fouda MM, El-Aassar M, Al-Deyab SS (2013) Antimicrobial activity of carboxymethyl chitosan/polyethylene oxide nanofibers embedded silver nanoparticles. Carbohyd Polym 92(2):1012–1017
17. Veerapandian M, Yun K (2011) Functionalization of biomolecules on nanoparticles: specialized for antibacterial applications. Appl Microbiol Biotechnol 90:1655–1667
18. Siripatrawan U, Kaewklin P (2018) Fabrication and characterization of chitosan-titanium dioxide nanocomposite film as ethylene scavenging and antimicrobial active food packaging. Food Hydrocoll 84:125–134
19. Rahman PM et al (2018) Chitosan/nano ZnO composite films: enhanced mechanical, antimicrobial and dielectric properties. Arab J Chem 11(1):120–127
20. Archana D et al (2013) In vivo evaluation of chitosan–PVP–titanium dioxide nanocomposite as wound dressing material. Carbohyd Polym 95(1):530–539
21. Lin D et al (2020) Preparation and characterization of TiO_2-Ag loaded fish gelatin-chitosan antibacterial composite film for food packaging. Int J Biol Macromol 154:123–133
22. Li Z et al (2018) Multifunctional cementitious composites modified with nano titanium dioxide: a review. Compos Part A Appl Sci Manuf 111:115–137
23. Ramesan M et al (2016) Preparation, characterization, electrical and antibacterial properties of sericin/poly (vinyl alcohol)/poly (vinyl pyrrolidone) composites. J Appl Polym Sci 133(24):43535
24. Javed R et al (2022) Diverse biotechnological applications of multifunctional titanium dioxide nanoparticles: an up-to-date review. IET Nanobiotechnol 16(5):171–189
25. Enescu D et al (2020) Evaluation of the specific migration according to EU standards of titanium from Chitosan/Metal complexes films containing TiO_2 particles into different food simulants. A comparative study of the nano-sized vs micro-sized particles. Food Packag Shelf Life 26:100579
26. Zhang X et al (2017) Preparation of chitosan-TiO_2 composite film with efficient antimicrobial activities under visible light for food packaging applications. Carbohyd Polym 169:101–107
27. Tao P et al (2013) Bulk transparent epoxy nanocomposites filled with poly (glycidyl methacrylate) brush-grafted TiO_2 nanoparticles. Polymer 54(6):1639–1646
28. Polu AR, Rhee H-W (2016) The effects of LiTDI salt and POSS-PEG (n= 4) hybrid nanoparticles on crystallinity and ionic conductivity of PEO based solid polymer electrolytes. Sci Adv Mater 8(5):931–940
29. El Fewaty NH, El Sayed A, Hafez R (2016) Synthesis, structural and optical properties of tin oxide nanoparticles and its CMC/PEG–PVA nanocomposite films. Polym Sci Ser A 58(6):1004–1016
30. Sundaramahalingam K et al (2019) Electrical properties of lithium bromide poly ethylene oxide/poly vinyl pyrrolidone polymer blend elctrolyte. Phys B Condens Matter 553:120–126
31. Dhatarwal P, Sengwa R (2021) Investigation on the optical properties of (PVP/PVA)/Al_2O_3 nanocomposite films for green disposable optoelectronics. Phys B Condens Matter 613:412989
32. Alshehawy AM et al (2021) Photoluminescence spectroscopy measurements for effective condition assessment of transformer insulating oil. Processes 9(5):732
33. El Askary A et al (2022) Optical, thermal, and electrical conductivity strength of ternary CMC/PVA/Er_2O_3 NPs nanocomposite fabricated via pulsed laser ablation. Phys B Condens Matter 637:413910
34. Morsi M et al (2018) Effect of lithium titanate nanoparticles on the structural, optical, thermal and electrical properties of polyethylene oxide/carboxymethyl cellulose blend. J Mater Sci: Mater Electron 29:15912–15925
35. Abdelghany A, Oraby A, Farea M (2019) Influence of green synthesized gold nanoparticles on the structural, optical, electrical and dielectric properties of (PVP/SA) blend. Phys B Condens Matter 560:162–173
36. Davis E, Mott N (1970) Conduction in non-crystalline systems V. Conductivity, optical absorption and photoconductivity in amorphous semiconductors. Philos Mag 22(179):0903–0922
37. Abdelghany A, Farea M, Oraby A (2021) Structural, optical, and electrical reinforcement of gamma-irradiated PEO/SA/Au NPs nanocomposite. J Mater Sci Mater Electron 32:6538–6549

38. Ismail KA et al (2022) Perspectives on composite films of chitosan-based natural products (Ginger, Curcumin, and Cinnamon) as biomaterials for wound dressing. Arab J Chem 15(4):103716
39. Helmy ET et al (2021) Novel green synthesis of S-doped TiO_2 nanoparticles using Malva parviflora plant extract and their photocatalytic, antimicrobial and antioxidant activities under sunlight illumination. Chemosphere 271:129524

Authors and Affiliations

Azzah M. Alghamdi[1] · I. Guizani[2] · E. M. Abdallah[3] · M. O. Farea[4] · M. A. Morsi[5,6] · Ibrahim A. Alhagri[7] · Talal F. Qahtan[8] · Ahmed N. Al-Hakimi[7] · Sadeq M. Al-Hazmy[7] · S. El-Sayed Saeed[7] · Abuzar E. A. E. Albadri[7]

✉ M. O. Farea
mhd.omar1984@gmail.com

[1] University of Jeddah, College of Science, Department of Physical Sciences, Jeddah, Saudi Arabia

[2] Physics Department, Faculty of Sciences and Arts in Qurayyat, Jouf University, Sakaka, Jouf, Saudi Arabia

[3] Department of Basic Sciences, Delta University for Science and Technology, Gamassa, Mansoura, Egypt

[4] Physics Department, Faculty of Science, Ibb University, Ibb, Yemen

[5] Physics Department, Faculty of Science, Taibah University, Al-Ula, Medina, Saudi Arabia

[6] Mathematical and Natural Sciences Department, Faculty of Engineering, Egyptian Russian University, Badr City, Cairo, Egypt

[7] Department of Chemistry, College of Sciences, Qassim University, 51452 Buraidah, Qassim, Saudi Arabia

[8] Physics Department, College of Science and Humanities in Al-Kharj, Prince Sattam Bin Abdulaziz University, 11942 Al-Kharj, Saudi Arabia